



## Predictions of air quality and challenges for eliminating air pollution during the 2022 Olympic Winter Games

Wenyi Yang<sup>a,f</sup>, Qizhong Wu<sup>b,e</sup>, Jie Li<sup>a,c,\*</sup>, Xueshun Chen<sup>a</sup>, Huiyun Du<sup>a</sup>, Zhe Wang<sup>a</sup>, Dongqing Li<sup>b</sup>, Xiao Tang<sup>a</sup>, Yele Sun<sup>a,c</sup>, Zhilan Ye<sup>a,c</sup>, Xiaole Pan<sup>a,c</sup>, Baozhu Ge<sup>a</sup>, Huansheng Chen<sup>a</sup>, Lianfang Wei<sup>a</sup>, Tao Wang<sup>a</sup>, Wei Wang<sup>d</sup>, Lili Zhu<sup>d</sup>, Jinyuan Xin<sup>a,c</sup>, Zifa Wang<sup>a,c</sup>

<sup>a</sup> State Key Laboratory of Atmospheric Boundary Layer Physics and Atmospheric Chemistry, Institute of Atmospheric Physics, Chinese Academy of Sciences, Beijing 100029, China

<sup>b</sup> College of Global Change and Earth System Science, Beijing Normal University, Beijing 100875, China

<sup>c</sup> College of Earth and Planetary Sciences, University of Chinese Academy of Sciences, Beijing 100049, China

<sup>d</sup> China National Environmental Monitoring Center, Beijing 100012, China

<sup>e</sup> Joint Center for Earth System Modeling and High Performance Computing, Beijing Normal University, Beijing 100875, China

<sup>f</sup> Center of Air Quality Simulation and System Analysis, Chinese Academy of Environmental Planning, Beijing 100012, China

### ARTICLE INFO

**Keywords:**  
Olympic Winter Games  
Air pollution  
Numerical model  
Source apportionment

### ABSTRACT

Scientifically and efficiently ensuring good air quality for important events is an issue of concern to the government. In addition to analysis based on historical data, advanced prediction before an event is essential for the government having ample time to take effective actions to improve air quality during the event period. Taking “the 2022 Olympic Winter Games (OWG)” as a typical case, a chemical transport model coupled with a tracer-tagged module was used to evaluate the air quality and source apportionment of ambient pollutants in the OWG host cities under historical and predicted meteorological conditions. Driven by the downscaling of meteorological fields from an operational real-time climate forecast system, the potential ability of air quality forecasting three months ahead was investigated, which was meaningful for designing control strategies. Sensitive simulations indicated that under unfavorable meteorological conditions, such as those during February 2014, both Beijing and Zhangjiakou faced a high risk of experiencing haze episodes, even based on current anthropogenic emission intensity. The contribution of the joint prevention and control region to Beijing and Zhangjiakou would become larger under worse meteorological conditions, which favor heavy air pollution. The source apportionment results indicated that strengthened emission control in cities including Beijing, Zhangjiakou and south of Beijing (Baoding, Langfang, Tianjin, and Tangshan) is effective for reducing haze episodes in the host cities. There is still a long way to make accurate daily fine particulate matter predictions on a seasonal-scale in advance; however, it could capture the trends in air quality in host cities around the OWG period three months ahead. The comparison of observations and predictions confirmed and highlighted the role of regional emission controls on the realization of the “OWG blue”.

### 1. Introduction

The 2022 Olympic Winter Games (OWG) was held in Beijing (BJ) and Zhangjiakou (ZJK), China, from February 4th to 20th, 2022 (<https://www.beijing2022.cn/>). To minimize potential health risks related to exposure to high concentration of ambient fine particulate matter

(PM<sub>2.5</sub>) (WHO, 2006; Henschel et al., 2012), the Chinese government proposed a series of measures to reduce the emissions of air pollutants and aimed to maintain the PM<sub>2.5</sub> concentration to achieve Chinese ambient air quality grade II standards (daily PM<sub>2.5</sub> concentration below 75 µg m<sup>-3</sup>) during the OWG. According to the long-term monitoring data of air pollutants released by the China National Environmental

\* Corresponding author at: State Key Laboratory of Atmospheric Boundary Layer Physics and Atmospheric Chemistry, Institute of Atmospheric Physics, Chinese Academy of Sciences, Beijing 100029, China.

E-mail address: [lijie8074@mail.iap.ac.cn](mailto:lijie8074@mail.iap.ac.cn) (J. Li).

Monitoring Center (CNEMC, <http://106.37.208.233:20035/>), the ambient PM<sub>2.5</sub> level in BJ and surrounding areas has displayed a declining trend in recent years. However, this region is still beset by wintertime haze episodes (Zhang et al., 2019).

To support the improvement of air quality for important events and potential air pollution episodes, a series of enhanced emission reduction measures should be implemented around certain areas in advance (Chen et al., 2015; Yang et al., 2019). Joint Prevention and Control of Air Pollution (JPCAP) policy has been applied to prevent heavy haze pollution for many years in China (Wang and Zhao, 2018). By using sensitivity simulation, Guo et al. (2016) found that the implementation of emission controls in BJ and surrounding regions resulted in reduction of 22% and 14% for PM<sub>2.5</sub> level in BJ, respectively, during the Asia-Pacific Economic Cooperation (APEC) China 2014. The consecutive blue-sky days during the OWG period confirmed that the JPCAP around the host cities was successful.

The determination of JPCAP boundaries involves many factors such as pollutant emissions, regional transport, economic structure, and environment carrying capacity (Xie et al., 2018; Zheng et al., 2018; Song et al., 2020; Wu et al., 2020; Sun et al., 2021; Zhang et al., 2021). Numerical simulation of air quality and source apportionment could provide scientific suggestions for deciding whether to adopt strict emission reduction measures and to develop more reasonable policies to minimize the conflict of interests between environmental protection and economic growth. The importance of different potential source regions to a certain region could be investigated according to historical meteorological conditions. Wang et al. (2021a) found that except for local emissions, the regional transport from central Hebei, Tianjin, and northern Hebei was important when the daily PM<sub>2.5</sub> concentration was  $>75 \mu\text{g m}^{-3}$  in BJ and ZJK during January 2015. Long-term air quality forecasting which has scarcely been conducted, should be helpful and essential for the government to have ample time to take effective actions to improve air quality during certain event periods.

In addition to anthropogenic emissions, meteorological conditions play a significant role in air quality by affecting the physical and chemical processes (including advection, diffusion, deposition, and chemical production) of pollutants (Leung et al., 2018; Zhai et al., 2019). Despite the changes in anthropogenic emissions, air pollutants in a certain receptor region were influenced by various contributions of different source regions under different meteorological conditions. Using Lagrangian transport and dispersion models and monitoring data, Zhang et al. (2022) estimated the contribution of different source regions to ZJK during February from 2015 to 2021 and found that the North China Plain and northern Shanxi Province were the main potential source regions and resulted in the increased PM<sub>2.5</sub> concentration in ZJK since 2018. Based on a fixed anthropogenic emission inventory, the influence of various meteorological conditions could be evaluated using a chemical transport model (Xu et al., 2020; Gong et al., 2021; Du et al., 2022). Comparison of simulated results under different meteorological conditions is helpful to highlight the challenges of environmental management during the OWG period.

In this study, a chemical transport model coupled with on-line tracer-tagged module was used to investigate the air quality and source-receptor relationship of PM<sub>2.5</sub> in 2022 OWG host cities. Seasonal-scale air quality forecasting driven by meteorological field downscaling from an operational real-time climate model was adopted to support JPCAP policy-making in advance. In addition, to present the prospects of challenges when designing emission control measures, sensitivity simulations were conducted under different meteorological conditions including an extremely unfavorable synoptic situation. Furthermore, the ability of long-term predictions for the trend in air quality was evaluated.

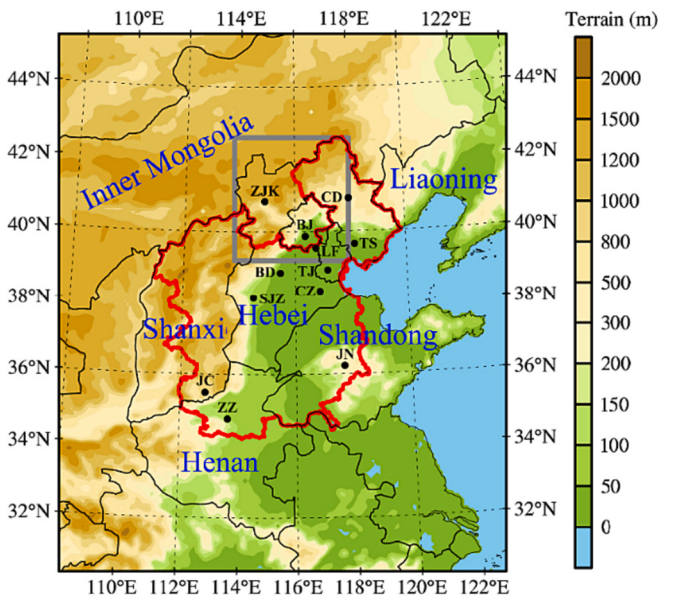


**Fig. 1.** The nested model domains for the NAQPMS. The gray rectangle denotes the inner domain. Beijing (BJ) and Zhangjiakou (ZJK) belong to the core control region, and the red line denotes the key joint control region. Blue text shows the provinces in or around the JPCAP region. Also shown are the topography (shaded) and twelve sites (black dots) selected to evaluate the model performance, including BJ, ZJK, Chengde (CD), Tangshan (TS), Langfang (LF), Tianjin (TJ), Baoding (BD), Shijiazhuang (SJZ), Cangzhou (CZ), Jinan (JN), Jincheng (JC), and Zhengzhou (ZZ). (For interpretation of the references to color in this figure legend, the reader is referred to the web version of this article.)

## 2. Method and data

### 2.1. Model description

The Nested Air Quality Prediction Modeling System (NAQPMS) is a 3-dimensional Eulerian chemical transport model that has been widely used in routine air quality forecasting by the Environmental Monitoring Center of many cities in China in the last decade (Wang et al., 2014; Chen et al., 2019; Chen et al., 2021).

The NAQPMS includes modules that address horizontal and vertical advection and diffusion, dry and wet deposition, and multiphase chemical reactions with terrain-following coordinates from the surface to 20 km. An accurate mass-conservative, peak-preserving advection algorithm and parameterized scheme of diffusion were implemented according to the approach proposed by Walcek and Aleksic (1998) and Byun and Dennis (1995), respectively. Aqueous chemistry and wet deposition schemes were based on the second generation of the Regional Acid Deposition Model (RADM2) (Stockwell et al., 1997). For gas-phase chemistry, the Carbon Bond Mechanism Z (CBM-Z) model (Zaveri and Peters, 1999) was implemented. The ammonia-sulfate-nitrate-chloride-sodium-water system was simulated using the thermodynamic equilibrium module ISORROPIA (Nenes et al., 1998). Secondary organic aerosol was calculated based on the volatility basis set (VBS) approach (Donahue et al., 2006; Koo et al., 2014). The heterogeneous chemistry module containing 14 species and 28 reactions was implemented to reproduce the mixing process between aerosols and gaseous pollutants (Li et al., 2018).

In addition, to evaluate the source-receptor relationship of PM<sub>2.5</sub>, an on-line tracer-tagged module that considers the effect of chemical nonlinearity was implemented in the NAQPMS. The apportionment of each species during the emission, physical and chemical processes was separately calculated. During the emissions-processing step, each species was categorized into different source regions and source categories. During physical processes including advection, diffusion and deposition

**Table 1**  
Sensitivity experiment configuration.

Experiment	Data to drive WRF model	Description
C-M2022	Real-time 9-month forecast of the CFSv2 released at 12 UTC on October 21, 2021	conducted >3 months ahead of the opening of the 2022 OWG to evaluate the ability of a seasonal-scale air quality prediction
F-M2021	FNL product from January 21 to February 28, 2021	preassessment of emission reductions based on the meteorological conditions in the last year
F-M2014	FNL product from January 21 to February 28, 2014	preassessment of emission reductions with extremely unfavorable meteorological conditions in recent years used to discuss the challenges for eliminating air pollution days
F-M2022	FNL product from January 21 to February 28, 2022	a retrospective prediction to assess the performance of the seasonal-scale air quality prediction in the C-M2022 case

processes, species do not change their chemical components but were transported physically. During chemical processes, referring to the algorithm proposed by Wagstrom et al. (2008), each secondary component was categorized directly according to specific precursor species. Detailed model descriptions and algorithms can be found in previous studies (Li et al., 2017; Wu et al., 2017).

The Weather Research and Forecasting (WRF) model (Skamarock et al., 2021), which could be run using interpolated data from an external analysis or forecast for real-data cases, was applied to provide the hourly meteorological field inputs to the NAQPMs. To provide the lateral and upper boundary conditions for the outermost domain, concentrations of several species were taken from the global chemistry transport model MOZART-v2.4 with a 2.8° horizontal spatial resolution (Hauglustaine et al., 1998).

## 2.2. Model setup and numerical experiments

Two nested domains with horizontal resolutions of 9 and 1 km were adopted: the outer domain covering the North China Plain and the inner domain focusing on BJ and ZJK (Fig. 1). In this study, the two host cities of OWG (BJ and ZJK) composed the core region of JPCAP, and >30 cities were regarded as key control regions (red line in Fig. 1). As shown in

Fig. S2, to precisely assess the regional source apportionment of pollutants, 43 geographical source regions, including BJ, ZJK, 35 cities among the key control regions, 5 regions in Inner Mongolia, Shanxi, Henan, Shandong, and Liaoning Province around the control region, and the other areas of the modeling domain, were investigated.

As mentioned above, the meteorological field inputs to NAQPMs were provided by the Weather Research and Forecasting (WRF) model. In this study, the different meteorological initial and boundary conditions to drive the WRF model for sensitivity experiments were taken from the National Centers for Environmental Prediction (NCEP) final (FNL) analysis data and an operational real-time forecast from the Climate Forecast System, version 2 (CFSv2).

The FNL product is from the Global Data Assimilation System (GDAS) and made with the model in the Global Forecast System (GFS). The FNL product used in this study has a horizontal resolution of 0.25° and is prepared operationally every six hours (<https://rda.ucar.edu/datasets/ds083.3/>).

Since the FNL product contains continuous real-time observations, it is typically used for historical simulations. For the CFSv2 data assimilation system in operations, there are four runs out to 9 months per day from the 00, 06, 12 and 18 UTC cycles. The initial conditions for these predicted products are obtained from the real time operational Climate Data Assimilation System, version 2 (CDASv2), which is the real time continuation of the Climate Forecast System Reanalysis (CFSR). Detailed model descriptions and evaluation can be found in Saha et al. (2014). The real time predicted CFSv2 product could be downloaded from the official site (<https://www.ncep.noaa.gov/data/climate-forecast-system/access/operational-9-month-forecast/>) and provided the opportunity for seasonal-scale numerical air quality forecasting in advance.

The anthropogenic emission inventories for different source categories (industrial, power plant, residential, and transportation) in China were based on the year 2018 developed by Tsinghua University. In this study, the modeling experiments for analysis were based on fixed anthropogenic emissions with varying meteorological conditions. As shown in Table 1, a control run using the predicted CFSv2 product, named C-M2022, and three sensitivity runs using FNL products were conducted. In the C-M2022 experiments, the 9-month forecast results of CFSv2 released at 12 UTC on October 21, 2021, were downloaded to drive the WRF model. The air quality forecast in the C-M2022 case was conducted >3 months ahead of the opening of the 2022 OWG in attempt to evaluate the ability of a seasonal-scale prediction to provide effective suggestions in advance to ensure good air quality for certain events.

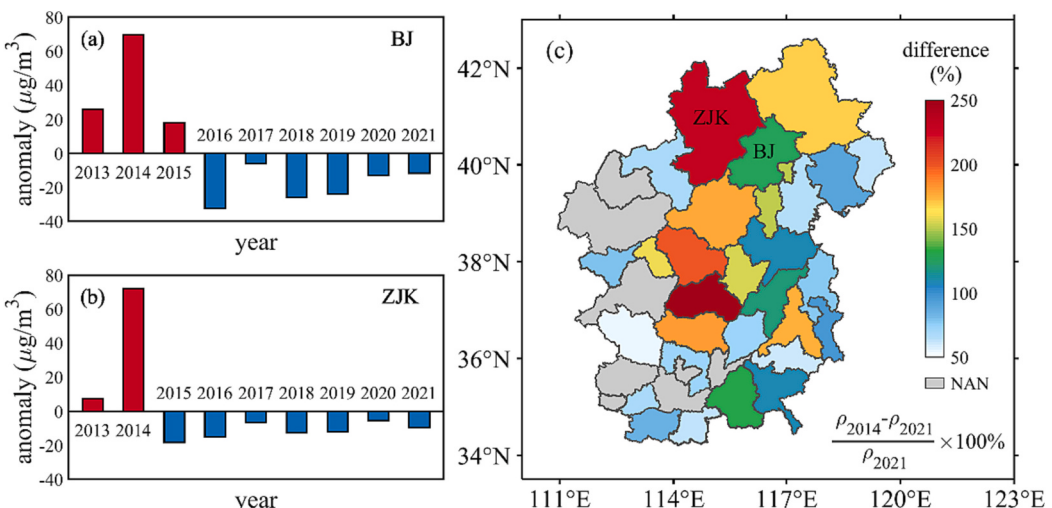


**Fig. 2.** Monthly (in February) PM<sub>2.5</sub> concentration anomalies from 2013 to 2021 in (a) BJ and (b) ZJK. (c) Relative difference between 2014 and 2021 in BJ, ZJK and other cities among key control regions (unit: %). Cities in gray indicate a lack of monitoring data for February 2014. The relative difference in Fig. 2c was obtained from  $(\rho_{2014} - \rho_{2021}) / \rho_{2021} \times 100\%$ , where  $\rho_{2014}$  and  $\rho_{2021}$  were the monitoring monthly mean concentrations of PM<sub>2.5</sub> in February 2014 and February 2021, respectively.

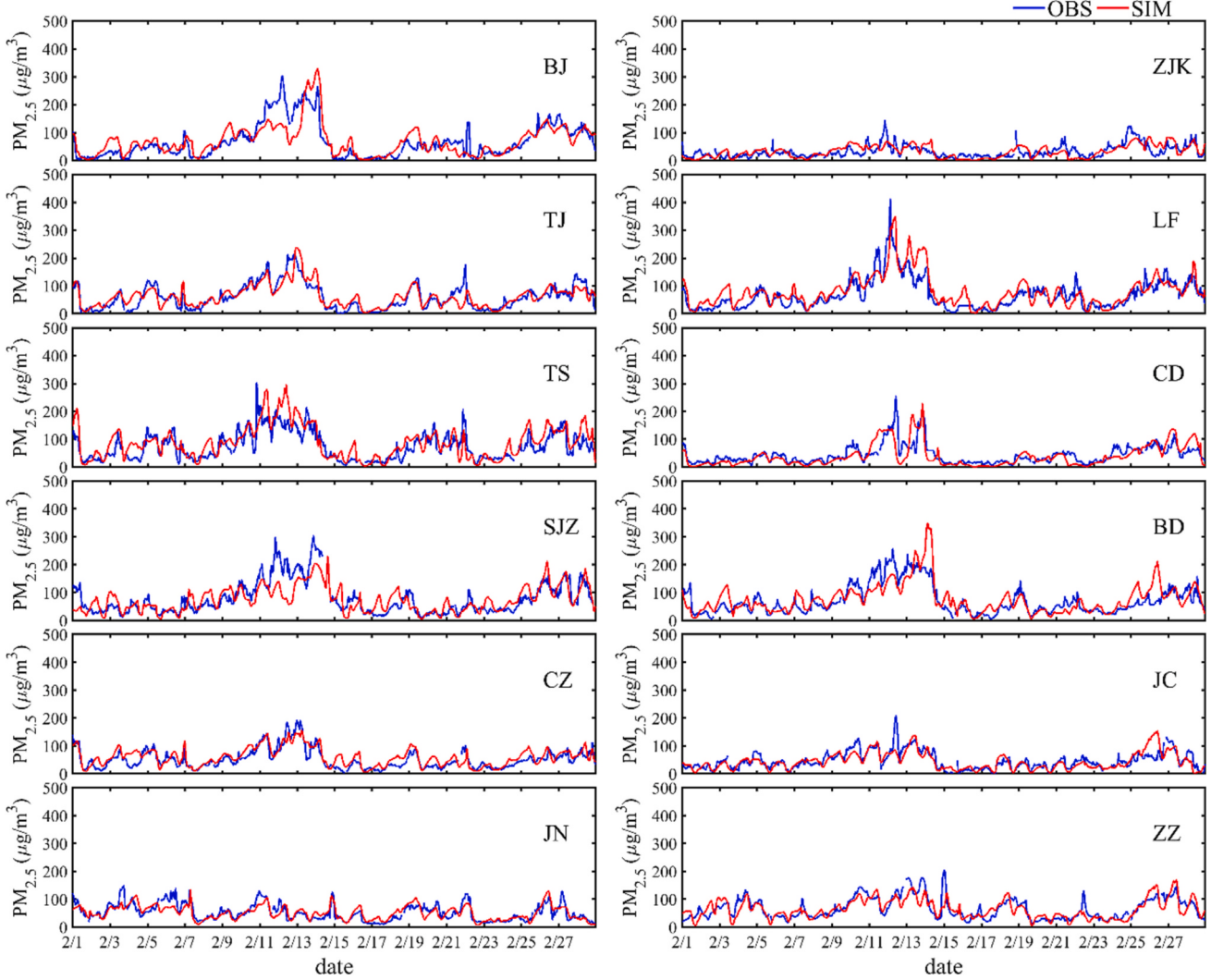


**Fig. 3.** Time series of the comparisons between hourly observed (OBS) and simulated (SIM) PM<sub>2.5</sub> concentrations for February 2021 (F-M2021 simulation) at twelve representative sites shown in Fig. 1.

Traditionally, the preassessment of emission reduction has been based on the meteorological conditions during the same period in last year or recent years. Therefore, the simulation during February 2021 driven by FNL products was conducted as the F-M2021 case. According to the historical monitoring data released by the CNEMC, monthly PM<sub>2.5</sub> concentration anomalies in BJ and ZJK in February from 2013 to 2021

were calculated. As shown in Fig. 2, the maximum positive concentration anomalies in BJ and ZJK both appeared in February 2014. In addition, the observed monthly mean PM<sub>2.5</sub> level in February 2014 was >50% higher than that in February 2021 within the JPCAP region (Fig. 2c). Although it is undeniable that the reduction in anthropogenic emissions contributed largely to the improvement in air quality, a

**Table 2**

Statistics between observed and simulated hourly PM<sub>2.5</sub> at twelve representative sites shown in Fig. 1 for February 2021. MO and MM represent the average of the observed and modeled PM<sub>2.5</sub> concentration (unit:  $\mu\text{g m}^{-3}$ ), respectively. N is the total effective number of paired observed/modeled values. The description of other statistical metrics can be found in the supplementary information (S1).

Site	MO $\mu\text{g m}^{-3}$	MM $\mu\text{g m}^{-3}$	N /	R /	RMSE $\mu\text{g m}^{-3}$	NMB %	NME %	MFB %	MFE %	IOA /
BJ	67.3	70.0	662	0.78	39.7	4.0	40.5	14.8	47.0	0.87
ZJK	31.6	31.6	665	0.58	20.1	0.1	49.8	-10.7	58.2	0.76
TJ	59.5	62.7	658	0.83	25.6	5.4	31.7	18.4	41.0	0.90
LF	67.1	80.1	666	0.84	34.2	19.4	38.6	21.6	43.2	0.90
TS	74.6	88.8	660	0.78	38.6	19.1	39.8	14.4	41.8	0.86
CD	43.3	38.8	669	0.73	27.6	-10.3	41.4	-31.3	52.7	0.84
SJZ	77.6	73.9	657	0.74	40.0	-4.9	37.4	-0.1	40.6	0.84
BD	70.8	75.7	668	0.74	38.2	6.9	38.7	8.0	39.6	0.85
CZ	51.8	60.2	666	0.82	22.1	16.2	33.2	18.1	36.0	0.89
JC	46.7	43.9	653	0.75	22.1	-6.1	32.1	-6.7	38.4	0.86
JN	53.0	51.6	666	0.76	19.6	-2.7	27.4	1.2	29.1	0.86
ZZ	66.5	64.5	664	0.76	25.5	-3.0	28.6	-1.4	32.1	0.86

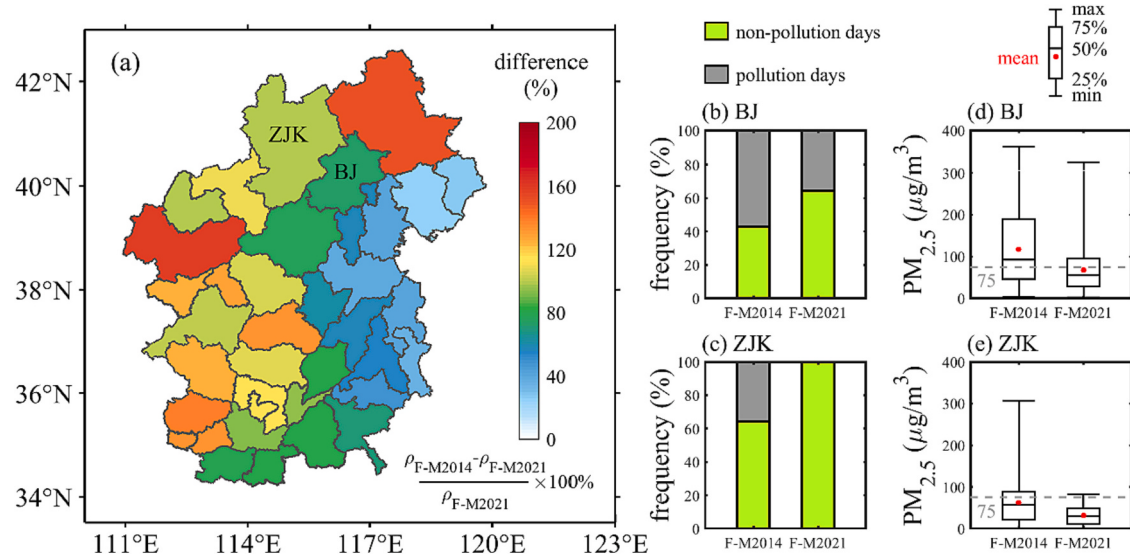


**Fig. 4.** The impacts of different meteorological conditions on PM<sub>2.5</sub> concentrations according to the F-M2021 and F-M2014 simulations. (a) The relative difference in the mean concentration in 2014 with 2021 as the base year in each city located in the joint control region. The frequency of pollution and nonpollution days in (b) BJ and (c) ZJK. Boxplots of hourly PM<sub>2.5</sub> concentration in (d) BJ and (e) ZJK. The relative difference in Fig. 2a was obtained from  $(\rho_{F\text{-M}2014} - \rho_{F\text{-M}2021}) / \rho_{F\text{-M}2021} \times 100\%$ , where  $\rho_{F\text{-M}2021}$  and  $\rho_{F\text{-M}2014}$  were the simulated monthly mean concentrations of PM<sub>2.5</sub> in F-M2021 and F-M2014, respectively.

simulation based on the FNL products of February 2014 (named F-M2021) was selected to represent the situation with extremely unfavorable meteorological conditions in recent years to discuss the risks outlined by the JPCAP. The setup of the F-M2022 simulation (including both the emission inventory and parameterization schemes) was the same as that of the C-M2022 simulation, except for the simulation period (from January 21 to February 28, 2022) and the meteorological conditions taken from the FNL products. The F-M2022 case was regarded as a retrospective prediction to assess the performance of the seasonal-scale air quality prediction in the C-M2022 case. To reduce the potential influence of initial conditions, the first 10 days were regarded as the spin-up period in each scenario.

### 3. Results and discussion

#### 3.1. Model performance

Since the fixed anthropogenic emission inventory used in this study did not take any potential reductions into account, the simulated PM<sub>2.5</sub> concentration in the F-M2021 case was selected to evaluate the NAQPMs model performance. Fig. 3 compares the hourly observed and simulated PM<sub>2.5</sub> concentrations for February 2021 at twelve representative sites (shown as black dots in Fig. 1). The real-time hourly measured total PM<sub>2.5</sub> mass was taken from the National Observation Network of Atmospheric Pollutants established by CNEMC. To provide a comprehensive picture of the model's ability to capture the magnitude of and variation in pollutant concentrations, several statistical metrics including the root mean square error (RMSE), correlation coefficient (R), index of agreement (IOA), normalized mean bias (NMB), normalized mean error (NME), mean fractional bias (MFB), and mean fractional error (MFE) were considered (Simon et al., 2012). A detailed description can be found in the supplementary information (S1).

As shown in Table 2, R and IOA ranged from 0.58 to 0.84 and 0.76 to 0.90, respectively. The simulation matched the trends of the variation in the observed hourly PM<sub>2.5</sub> level. The NMB, NME, MFB, and MFE were in percentage units and represent normalized values based on observations. The NMB ranged from -10.3% to 19.4%, and the NME ranged from 27.4% to 49.8%. As suggested by Boylan and Russell (2006), the assessment criteria were set to MFB  $\leq \pm 60\%$  and MFE  $\leq 75\%$  for the PM<sub>2.5</sub> simulations. MFB ranged between -31.3% and 21.6%, and MFE

ranged between 29.1% and 58.2%. From February 11 to 13, there were still biases between the simulations and observations in BJ, BD and SJZ. Previous studies (Li and Han, 2016; Chang et al., 2019) found that regional transport from southern Hebei Province along the base of the Taihang Mountains to the downstream regions was important when haze episodes occurred in BJ. These acceptable biases along the pollution transport pathways might be due to uncertainties in the simulated meteorological fields, anthropogenic emission inventories, and incomplete chemical mechanisms used in the numerical model. Fig. S3 shows the distribution of the statistical metrics for observed and simulated PM<sub>2.5</sub> in the core and key control regions. Additionally, Fig. S4 shows the MFB and MFE values at 167 sites located in Beijing, Tianjin, Hebei Province, Shanxi Province, Shandong Province, and Henan Province in the F-M2021 case. Except for that at 3 sites in Shanxi Province, the PM<sub>2.5</sub> model performance was acceptable (MFB  $\leq \pm 60\%$  and MFE  $\leq 75\%$ ) or good (MFB  $\leq \pm 30\%$  and MFE  $\leq 50\%$ ) for regulatory applications.

In general, the spatial and temporal variations in the PM<sub>2.5</sub> level during February 2021 in the control region were captured well by the NAQPMs model. All the statistical values met the criteria for satisfactory performance. The results provided confidence in the source-receptor relationship analysis, which was expected to prioritize cities among the control regions.

#### 3.2. Influences of interannual variation in meteorological conditions

As mentioned above, the comparison between the F-M2021 and F-M2014 simulations could explain the impacts of meteorological conditions on PM<sub>2.5</sub> pollution. The relative difference for each city shown in Fig. 4a was obtained from  $(\rho_{F\text{-M}2014} - \rho_{F\text{-M}2021}) / \rho_{F\text{-M}2021} \times 100\%$ , where  $\rho_{F\text{-M}2021}$  and  $\rho_{F\text{-M}2014}$  were the monthly mean PM<sub>2.5</sub> concentrations in the F-M2021 and F-M2014 simulations, respectively. With fixed anthropogenic emissions (base year 2018), the relative difference exceeded 25% among the control region under unfavorable meteorological conditions. The PM<sub>2.5</sub> level in the southwestern part of the JPCAP region was largely affected by the meteorological conditions in 2014, with a positive change ranging from 80% to 160% compared with the F-M2021 simulation.

As shown in Fig. 1, BJ is surrounded by mountains to the north, west and northeast, with the terrain height tending to gradually decrease from northwest to southeast. With the blocking of such topography,

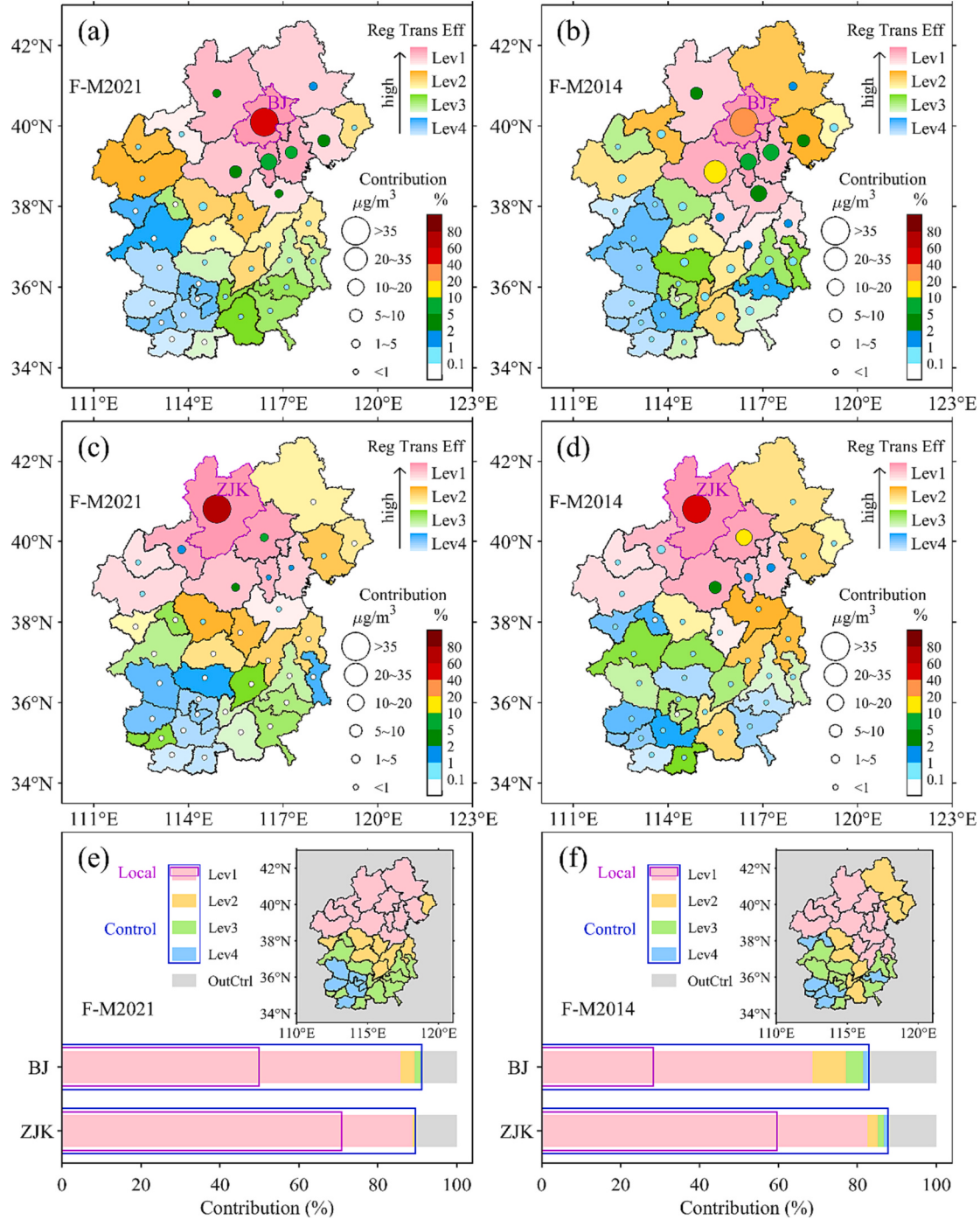


**Fig. 5.** The importance of source cities among the JPCAP region to BJ and ZJK in the F-M2021 and F-M2014 simulations under high PM<sub>2.5</sub> conditions (with hourly PM<sub>2.5</sub> levels in the highest quartile). (a) BJ and (c) ZJK as the receptor city in the F-M2021 simulation and (b) BJ and (d) ZJK as the receptor city in the F-M2014 simulation. The shaded color of each source city represents the level of control priority. The size of the circle shows the mean contribution of PM<sub>2.5</sub> concentration (unit:  $\mu\text{g m}^{-3}$ ), and the color of the circle demonstrates the relative contribution (unit: %). (e) and (f) show the contribution of different classified regions to BJ and ZJK in the F-M2021 and F-M2014 simulations, respectively. In addition, purple and blue rectangles indicate the contributions from the local and entire JPCAP regions, respectively. (For interpretation of the references to color in this figure legend, the reader is referred to the web version of this article.)

continuous weak southerly winds from polluted industrial source regions under stable weather conditions in wintertime could lead to heavy PM<sub>2.5</sub> pollution events in BJ (Guo et al., 2014; Quan et al., 2020; Xiao et al., 2020). For BJ and ZJK, the worsening conditions could result in the monthly mean PM<sub>2.5</sub> level increasing by approximately 75% and 99%, respectively.

According to the objectives for environmental safeguarding of the OWG, pollution days were defined as occasions with daily mean PM<sub>2.5</sub>

concentrations exceeding 75  $\mu\text{g m}^{-3}$  (Chinese ambient air quality grade II standards) in this study. The frequency of pollution days in BJ and ZJK in the F-M2014 simulation was higher than that in the F-M2014 simulations, especially in ZJK (Fig. 4b-c). The boxplot shown in Fig. 4d-e demonstrates that under the meteorological conditions of February 2014, the proportion of hourly PM<sub>2.5</sub> concentrations exceeding 75  $\mu\text{g m}^{-3}$  would reach >50% and 25% in BJ and ZJK, respectively.

A series of stringent actions have been implemented to improve air

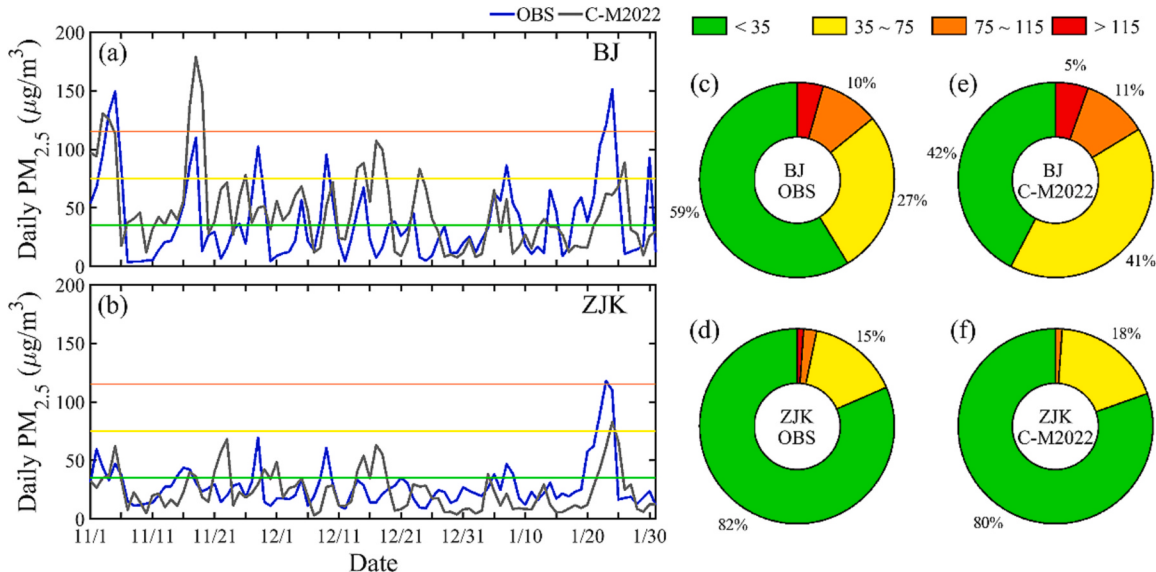


**Fig. 6.** Comparisons between observed (OBS) and predicted (C-M2022) daily PM<sub>2.5</sub> concentrations from November 1st, 2021 to January 31st, 2022. Time series of daily PM<sub>2.5</sub> in (a) BJ and (b) ZJK. The pie charts show the ratio of observed (c-d) and predicted (e-f) daily PM<sub>2.5</sub> concentrations under different levels in BJ and ZJK, respectively.

quality in recent years, and many previous studies (Zhai et al., 2019; Zhang et al., 2019; Gao et al., 2020) have confirmed the effectiveness of emission reduction actions for decreasing PM<sub>2.5</sub> levels in China in the long term. However, for certain periods, extremely unfavorable meteorological conditions still have a large chance of resulting in heavy haze episodes at a regional scale, which requires the government to put great effort into developing and implementing emission control measures.

### 3.3. Source-receptor relationship under different meteorological conditions

As mentioned above, 43 source emission regions including 37 individual cities in the JPCAP region, were tagged in this study (Fig. S2). According to the detailed administrative division, the regional transport efficiency, which indicates the impact of per unit emissions on the contribution of PM<sub>2.5</sub>, could be tracked separately. The regional transport efficiency was defined as the quotient of the PM<sub>2.5</sub> contribution from one source region to a certain receptor region to the total amount of primary emissions including primary PM<sub>2.5</sub>, black carbon, organic carbon, SO<sub>2</sub>, NO<sub>x</sub> and NH<sub>3</sub> in that source region. By sorting the values of regional transport efficiency from high to low, four levels of control priority among the JPCAP region were identified. The control priority of these cities decreased with descending quartiles. Specifically, cities in the first, second, third, and fourth quartiles of regional transport efficiency values were regarded as being Lev1, Lev2, Lev3 and Lev4 control priorities, which are shown in pink, orange, green and blue in Fig. 5a-d, respectively.

The characteristics of source apportionment among the JPCAP region under high PM<sub>2.5</sub> conditions could provide recommendations for policy-making. Since the concentration of PM<sub>2.5</sub> in ZJK was maintained at a low level (mostly below 75 µg m<sup>-3</sup>) in the F-M2021 simulation, the high PM<sub>2.5</sub> situation was regarded as the hourly PM<sub>2.5</sub> level in the highest quartile for each receptor city. Fig. 5a-d presents the importance of source cities among the JPCAP region to BJ and ZJK in the F-M2021 and F-M2014 simulations under high PM<sub>2.5</sub> conditions. Among the 37 cities in the JPCAP region, self-contribution accounted for the most in both BJ and ZJK. Compared with F-M2021 simulation, regional transport from adjacent cities became more important in the F-M2014 simulation. Under the meteorological conditions of February 2014, cities located south of BJ including BD, LF, TJ, and CZ, contributed

substantially to the PM<sub>2.5</sub> concentration in BJ, accounting for approximately 13%, 8%, 6%, and 4%, respectively. The self-contribution of BJ was reduced to approximately 30% in the F-M2014 simulation and remained at approximately 50% in the F-M2021 simulation. However, local emissions played a more dominant role in ZJK than in BJ. Compared with the F-M2021 simulation, even though the self-contribution of ZJK decreased >10% in the F-M2014 simulation, it still accounted for approximately 60% of the PM<sub>2.5</sub> level in ZJK.

Regarding BJ and ZJK as individual receptor cities, different source cities in the JPCAP region might be assigned to different levels of control priority. When taking BJ and ZJK as a whole receptor, a higher level was selected as the entire control priority for each source site (Fig. 5e-f). For example, in the F-M2021 simulation, TS was in Lev1 and Lev2 for BJ (Fig. 5a) and ZJK (Fig. 5c), respectively, and was finally regarded as a Lev1 priority during the joint control action (Fig. 5e). In general, the influence of the entire JPCAP region on BJ and ZJK reached approximately 80% to 90% in both the F-M2021 and F-M2014 simulations. Although long-distance transport from Lev3 and Lev4 cities could not be ignored under unfavorable meteorological conditions, the total contribution of Lev1 cities still dominated the PM<sub>2.5</sub> level in BJ and ZJK. Compared with the average situation (Fig. S6), the characteristics of the importance of source contributors to BJ and ZJK under high PM<sub>2.5</sub> conditions were similar except that regional transport had a slightly larger impact on the PM<sub>2.5</sub> concentration of BJ and ZJK.

Therefore, strengthened emission control measures taken within the whole JPCAP region are important for this region to improve the overall air quality in the long term or to reduce air pollution during certain haze episodes. However, distinguishing the control priority for different source regions and then enhancing the emission reduction measures in regions with high control priority are efficient means to focus on a specified receptor region.

### 3.4. Predictions for the air quality of BJ and ZJK around the OWG period

Based on the meteorological conditions that were downscaled from the forecasting of the CFSv2 climate model, a C-M2022 simulation was conducted to predict the air quality during the OWG period. To avoid the impact of emission reduction on air quality during the OWG period, the observed and predicted PM<sub>2.5</sub> concentrations from November 1st, 2021, to January 31st, 2022, were compared to evaluate the model

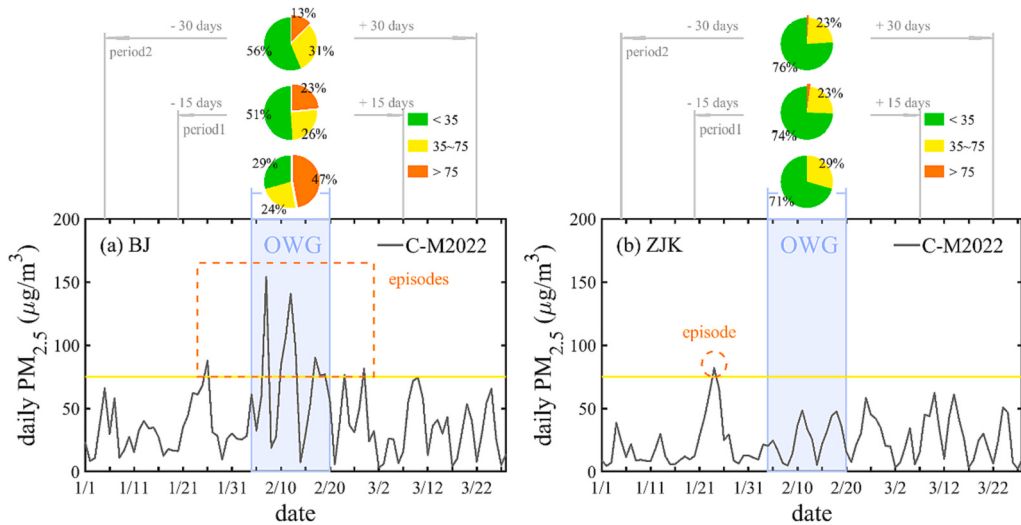


**Fig. 7.** Forecast for daily PM<sub>2.5</sub> concentrations in (a) BJ and (b) ZJK from January 1st to March 27th, 2022. The pie charts show the ratio of different daily PM<sub>2.5</sub> levels during the OWG period and 15 days and 30 days before and after the OWG period.

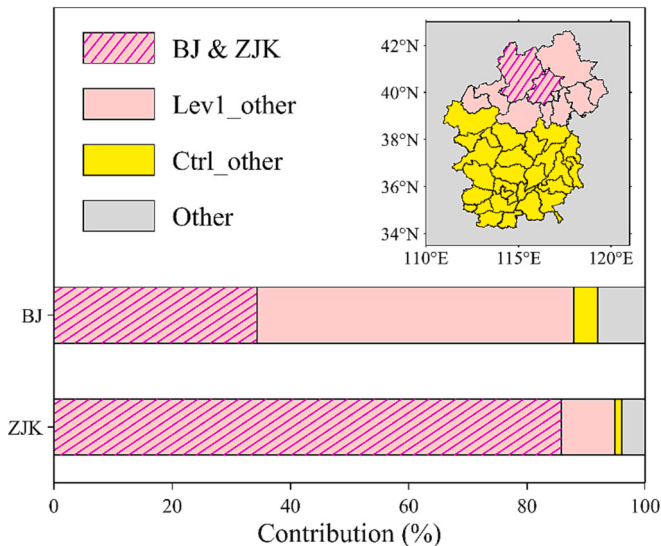


**Fig. 8.** Contribution of different source regions to BJ and ZJK under the predicted haze episodes (daily PM<sub>2.5</sub> concentration  $>75 \mu\text{g m}^{-3}$ ) in BJ during the OWG period in the C-M2022 case.

performance. Hourly observed and predicted PM<sub>2.5</sub> concentrations were averaged from the monitoring sites listed in the National Observation Network of Atmospheric Pollutants released by the CNEMC for BJ and ZJK, respectively. As shown in Fig. 6, the simulated nonpollution days (daily PM<sub>2.5</sub> concentration below 75  $\mu\text{g m}^{-3}$ ) accounted for 83% and 98% in BJ and ZJK, respectively, from November 2021 to January 2022. These results match the observed nonpollution days proportion of 86% and 97% in BJ and ZJK, respectively. Fig. 6a shows that the forecast for daily PM<sub>2.5</sub> in BJ is overestimated to some extent at low PM<sub>2.5</sub> concentrations, especially below 20  $\mu\text{g m}^{-3}$ . Generally, the seasonal-scale air quality forecast (C-M2022) had the ability to predict the trend of PM<sub>2.5</sub> variation in BJ and ZJK around the OWG period.

Considering the uncertainty of the meteorology conditions downscaling from climate forecasting, Fig. 7 shows the predicted daily PM<sub>2.5</sub> concentrations in BJ and ZJK about one month before and after the OWG (from January 1st to March 27th, 2022). According to the forecast, the air quality in ZJK was much better than that in BJ, and BJ was likely to experience several pollution episodes around the OWG period. During

the OWG period, 15 days and 30 days before and after the OWG period, the possible proportions of pollution days were 46%, 23% and 13%, respectively. It is imperative to prepare effective control measures to address the high risks of haze episodes in Beijing during the OWG period.

Based on the method mentioned above (Section 3.3), control priorities for cities in the JPCAP region were obtained by taking BJ and ZJK as a whole receptor. Fig. 8 shows the average contribution of the four grouped source regions to BJ and ZJK when the predicted daily PM<sub>2.5</sub> concentration exceeds 75  $\mu\text{g m}^{-3}$  in BJ. The four grouped regions included the total contribution of BJ and ZJK, cities in Lev1 except for BJ and ZJK, cities in the JPCAP region except for those in Lev1, and areas outside the JPCAP region. For ZJK, local emissions dominated the PM<sub>2.5</sub> level, and the total contribution of ZJK and BJ reached approximately 86%. The high PM<sub>2.5</sub> pollution that occurred in BJ was largely impacted by regional transport from other cities in the Lev1 control priority (accounting for approximately 53%), especially from the south and east of BJ including BD, LF, TJ, and TS. Considering that local emissions contributed  $>30\%$  to PM<sub>2.5</sub> pollution in BJ, the enhanced emission reduction measures in BJ, BD, LF, TJ, and TS deserve special consideration.

### 3.5. Prospects of the long-range prediction of air quality

As shown in Section 3.1, the NAQPMs model could generally reproduce the PM<sub>2.5</sub> concentration well using the meteorological fields driven by the FNL products. Comparison between C-M2022 and F-M2022 could provide a better understanding of the reliability of seasonal-scale air quality predictions based on climate forecast models. The evaluation of simulated PM<sub>2.5</sub> concentrations in both C-M2022 and F-M2022 in BJ and ZJK from January 27th to February 28th, 2022 was analyzed. As shown in Fig. 9a-b, the probability density function (PDF) of hourly PM<sub>2.5</sub> concentrations in BJ and ZJK displayed a similar distribution pattern in the seasonal-scale prediction (C-M2022) and retrospective simulation (F-M2022). Fig. 9c-d shows the time series of daily mean observed and simulated PM<sub>2.5</sub> in BJ and ZJK. Compared with the F-M2022 simulation, the C-M2022 simulation overestimated the PM<sub>2.5</sub> level in BJ. Additionally, comparison of the 3-day moving averages of the PM<sub>2.5</sub> concentration (Fig. 9e-f) showed that the C-M2022 simulation successfully predicted the trend of air quality in BJ and ZJK around the OWG period three months ahead. Considering the uncertainty in climate forecast models, it is difficult to predict the daily PM<sub>2.5</sub> level precisely at the seasonal scale.

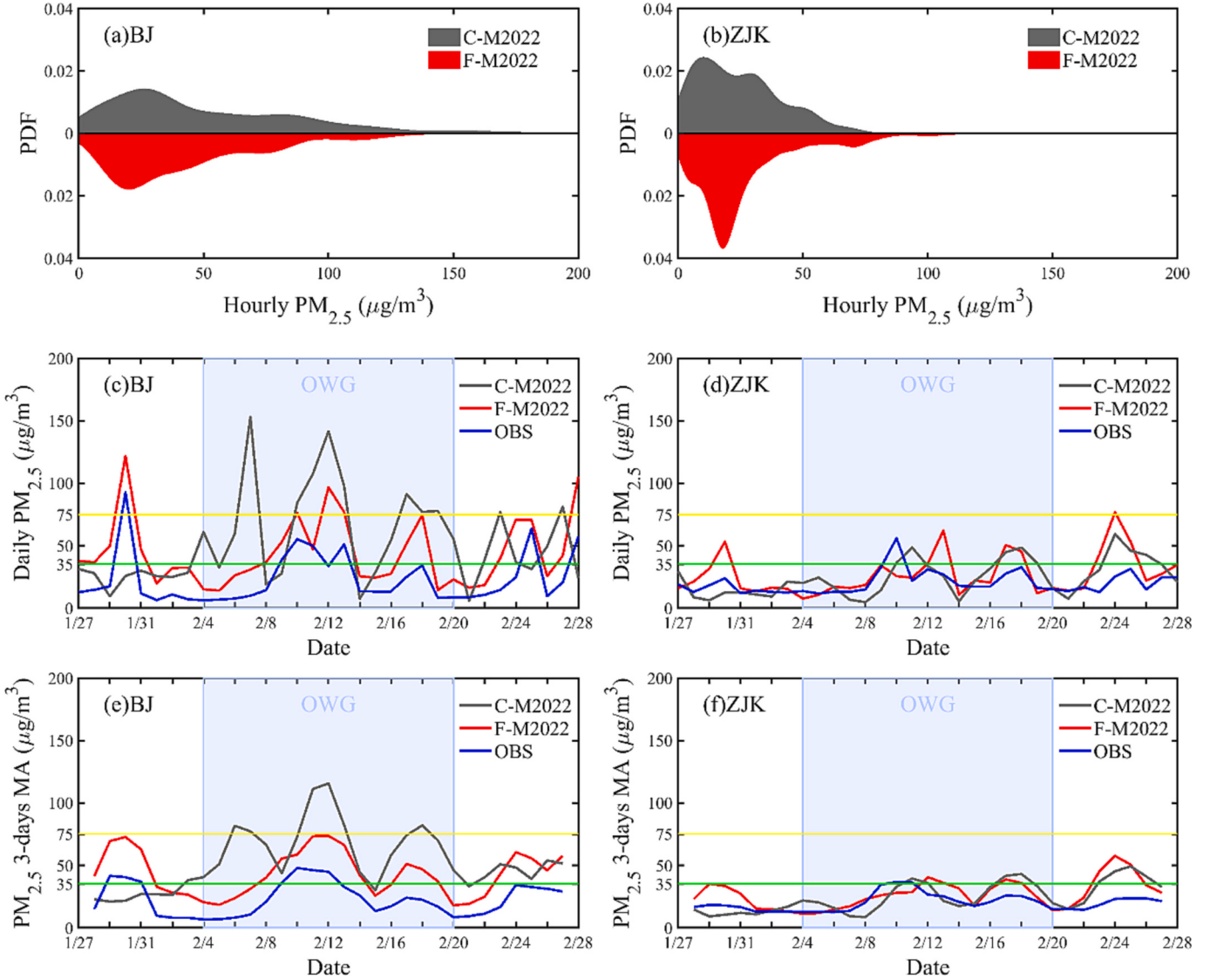


**Fig. 9.** Probability density function (PDF) of simulated (C-M2022 and F-M2022) hourly PM<sub>2.5</sub> concentrations (a-b). The time series of observed (OBS) and simulated (C-M2022 and F-M2022) daily PM<sub>2.5</sub> concentrations (c-d) and 3-day moving averages (MA) of PM<sub>2.5</sub> concentrations (e-f) in BJ and ZJK from January 27th to February 28th, 2022.

However, the model performance gives the confidence of the trend forecast of air quality for a period lasting for several days over the North China Plain in wintertime. Long-term air quality prediction would be useful to provide scientific recommendations for developing emission control measures a few months in advance.

The whole world has suffered from the COVID-19 pandemic during the past three years. A series of lockdown measures have been implemented nationwide in China to control the spread of the virus since late January 2020. By using a bottom-up approach, Zheng et al. (2021) estimated that the largest monthly emission change from 2019 to 2020 occurred in February with the emission of each air pollutant decreasing >20% in 2020, which was mainly contributed by the industry and transportation sectors. Many studies (Wang et al., 2020a; Wang et al., 2021b) have investigated the impacts of emission reduction on air quality in China during the lockdown period. Unfortunately, several haze episodes occurred in Beijing and the surrounding region during February 2020. Previous studies have shown that the benefits of anthropogenic emission reductions are overwhelmed by adverse meteorological conditions based on sensitive air quality simulations (Sulaymon et al., 2021; Wang et al., 2020b). There is no doubt that the declining trend of emissions could help improve air quality in the long

term. Since the emission inventory was based on the year 2018, none of the emission reductions is considered in this study. The gap between the observation and F-M2022 simulation indicated that the implementation of emission control measures ensured blue-sky days in the host cities during the OWG period.

#### 4. Conclusions

Comparison of sensitivity simulations indicated that the contribution of regional transport became more important under worse meteorological conditions in BJ and ZJK. The entire JPCAP region accounted for >80% or even >90% of the PM<sub>2.5</sub> level in BJ and ZJK in the C-M2022, F-M2021, and F-M2014 simulation, which confirmed the necessity of cooperative mechanisms for emission reduction.

Comparison between the results of the C-M2022 and F-M2022 simulation showed that the trend forecast of daily air quality in BJ and ZJK during the 2022 OWG period made 3 months ahead was successfully captured in this study. It is possible to provide useful and scientific recommendations for developing emission control measures for events lasting several days over the North China Plain in wintertime a few months in advance.

The simulations showed that BJ would face a high risk of suffering from several pollution episodes with daily PM<sub>2.5</sub> concentrations exceeding 75 µg m<sup>-3</sup> during the OWG period. However, the blue-sky days demonstrated the great efforts governments have made to realize the goal of eliminating pollution days in both BJ and ZJK during the whole OWG period.

### CRediT authorship contribution statement

**Wenyi Yang:** Conceptualization, Investigation, Writing – original draft. **Qizhong Wu:** Data curation. **Jie Li:** Conceptualization, Methodology. **Xueshun Chen:** Writing – original draft. **Huiyun Du:** Validation. **Zhe Wang:** Data curation. **Dongqing Li:** Data curation. **Xiao Tang:** Resources. **Yele Sun:** Resources. **Zhilan Ye:** Visualization. **Xiaole Pan:** Resources. **Baozhu Ge:** Resources. **Huansheng Chen:** Visualization. **Lianfang Wei:** Visualization. **Tao Wang:** Validation. **Wei Wang:** Resources. **Lili Zhu:** Resources. **Jinyuan Xin:** Resources. **Zifa Wang:** Supervision.

### Declaration of competing interest

The authors declare that they have no known competing financial interests or personal relationships that could have appeared to influence the work reported in this paper.

### Data availability

Data will be made available on request.

### Acknowledgments

This study was supported by the National Natural Science Foundation of China (No. 92044302, No.42377105, No.42207133), the National Key Research and Development Program of China (Grants No.2022YFC3700703), the Strategic Priority Research Program of the Chinese Academy of Sciences (Grant No. XDA19040202), and the Key Research and Development Program of Shanxi Province (202202090301023). We thank the National Key Scientific and Technological Infrastructure project “Earth System Science Numerical Simulator Facility” (EarthLab). We thank Prof. Shuxiao Wang at Tsinghua University for providing the anthropogenic emission inventory.

### Appendix A. Supplementary data

Supplementary data to this article can be found online at <https://doi.org/10.1016/j.atmosres.2024.107225>.

### References

- Boylan, J.W., Russell, A.G., 2006. PM and light extinction model performance metrics, goals and criteria for three-dimensional air quality models. *Atmos. Environ.* 40 (26), 4946–4959.
- Byun, D.W., Dennis, R., 1995. Design artifacts in Eulerian air-quality models -evaluation of the effects of layer thickness and vertical profile correction on surface ozone concentrations. *Atmos. Environ.* 29, 105–126.
- Chang, X., Wang, S., Zhao, B., Xing, J., Liu, X., Wei, L., Song, Y., Wu, W., Cai, S., Zheng, H., Ding, D., Zheng, M., 2019. Contributions of inter-city and regional transports to PM<sub>2.5</sub> concentrations in the Beijing-Tianjin-Hebei region and its implications on regional joint air pollution control. *Sci. Total Environ.* 660, 1191–1200.
- Chen, H., Li, J., Ge, B., Yang, W., Wang, Z., Huang, S., Wang, Y., Yan, P., Li, J., Zhu, L., 2015. Modeling study of source contributions and emergency control effects during a severe haze episode over the Beijing-Tianjin-Hebei area. *Sci. China Chem.* <https://doi.org/10.1007/s11426-015-5458-y>.
- Chen, X., Yang, W., Wang, Z., Li, J., Hu, M., An, J., Wu, Q., Wang, Z., Chen, H., Wei, Y., Du, H., Wang, D., 2019. Improving new particle formation simulation by coupling a volatility-basis set (VBS) organic aerosol module in NAQPMS+APM. *Atmos. Environ.* 204, 1–11.
- Chen, X., Yu, F., Yang, W., Sun, Y., Chen, H., Du, W., Zhao, J., Wei, Y., Wei, L., Du, H., Wang, Z., Wu, Q., Li, J., An, J., Wang, Z., 2021. Global-regional nested simulation of particle number concentration by combining microphysical processes with an evolving organic aerosol module. *Atmos. Chem. Phys.* 21, 9343–9266.
- Donahue, N.M., Robinson, A.L., Stanier, C.O., Pandis, S.N., 2006. Coupled partitioning, dilution, and chemical aging of semivolatile organics. *Environ. Sci. Technol.* 40, 2635–2643.
- Du, H., Li, J., Wang, Z., Chen, X., Yang, W., Sun, Y., Xin, J., Pan, X., Wang, W., Ye, Q., Dao, X., 2022. Assessment of the effect of meteorological and emission variations on winter PM<sub>2.5</sub> over the North China Plain in the three-year action plan against air pollution in 2018–2020. *Atmos. Res.* 280, 106395.
- Gao, M., Liu, Z., Zheng, B., Ji, D., Sherman, P., Song, S., Xin, J., Liu, C., Wang, Y., Zhang, Q., Xing, J., Jiang, J., Wang, Z., Carmichael, G.R., McElroy, M.B., 2020. China's emission control strategies have suppressed unfavorable influences of climate on wintertime PM<sub>2.5</sub> concentrations in Beijing since 2002. *Atmos. Chem. Phys.* 20, 1497–1505.
- Gong, S., Liu, H., Zhang, B., He, J., Zhang, H., Wang, Y., Wang, S., Zhang, L., Wang, J., 2021. Assessment of meteorology vs. control measures in the China fine particulate matter trend from 2013 to 2019 by an environmental meteorology index. *Atmos. Chem. Phys.* 21, 2999–3013.
- Guo, S., Hu, M., Zamora, M., Peng, J., Shang, D., Zheng, J., Du, Z., Wu, Z., Shao, M., Zeng, L., Molina, M., Zhang, R., 2014. Elucidating severe urban haze formation in China. *P. Natl. Acad. Sci. USA* 111, 17373–17387.
- Guo, J., He, J., Liu, H., Miao, Y., Liu, H., Zhai, P., 2016. Impact of various emission control schemes on air quality using WRF-Chem during APEC China 2014. *Atmos. Environ.* 140, 311–319.
- Hauglustaine, D.A., Brasseur, G.P., Walters, S., Rasch, P.J., Muller, J.F., Emmons, L.K., Carroll, M.A., 1998. MOZART, a global chemical transport model for ozone and related chemical tracers. 2. Model results and evaluation. *J. Geophys. Res.-Atmos.* 103 (D21), 28291–28335.
- Henschel, S., Atkinson, R., Zeka, A., Le Tertre, A., Analitis, A., Katouyanni, K., Chanel, O., Pascal, M., Forsberg, B., Medina, S., Goodman, P., 2012. Air pollution interventions and their impact on public health. *Int. J. Public Health* 57 (5), 757–768.
- Koo, B., Knipping, E., Yarwood, G., 2014. 1.5-Dimensional basis set approach for modeling organic aerosol in CAMx and CMAQ. *Atmos. Environ.* 95, 158–164.
- Leung, D., Tai, A.P.K., Mickley, L.J., Moch, J.M., van Donkelaar, A., Shen, L., Martin, R. V., 2018. Synoptic meteorological modes of variability for fine particulate matter (PM<sub>2.5</sub>) air quality in major metropolitan regions of China. *Atmos. Chem. Phys.* 18, 6733–6748.
- Li, J., Han, Z., 2016. A modeling study of severe winter haze events in Beijing and its neighboring regions. *Atmos. Res.* 170, 87–97.
- Li, J., Du, H., Wang, Z., Sun, Y., Yang, W., Li, J., Tang, X., Fu, P., 2017. Rapid formation of a severe regional winter haze episode over a megacity cluster on the North China Plain. *Environ. Pollut.* 223, 605–615.
- Li, J., Chen, X., Wang, Z., Du, H., Yang, W., Sun, Y., Hu, B., Li, J., Wang, W., Wang, T., Fu, P., Huang, H., 2018. Radiative and heterogeneous chemical effects of aerosols on ozone and inorganic aerosols over East Asia. *Sci. Total Environ.* 622–623, 1327–1342.
- Nenes, A., Pandis, S.N., Pilinis, C.A., 1998. ISORROPIA: a New Thermodynamic Equilibrium Model for Multiphase Multicomponent Inorganic Aerosols. *Aquat. Geochim.* 4 (1), 123–152.
- Saha, S., Moorthi, S., Wu, X., Wang, J., Nadiga, S., Tripp, P., Behringer, D., Hou, Y., Chuang, H., Iredell, M., Ek, M., Meng, J., Yang, R., Peña Mendez, M., van den Dool, H., Zhang, Q., Wang, W., Chen, M., Becker, E., 2014. The NCEP climate Forecast System Version 2. *J. Clim.* 27, 2185–2208.
- Simon, H., Baker, K.R., Phillips, S., 2012. Compilation and interpretation of photochemical model performance statistics published between 2006 and 2012. *Atmos. Environ.* 61, 124–139.
- Skamarock, W.C., Klemp, J.B., Dudhia, J., Gill, J.D.O., Liu, Z., Berner, J., Huang, X., 2021. A Description of the Advanced Research WRF Version 4.3 (No. NCAR/TN-556 +STR). <https://doi.org/10.5065/1dfh-6p97>.
- Song, Y., Li, Z., Yang, T., Xia, Q., 2020. Does the expansion of the joint prevention and control areas improve the air quality? Evidence from China's Jing-Jin-Ji region and surrounding areas. *Sci. Total Environ.* 706, 136034.
- Stockwell, W.R., Kirchner, F., Kuhn, M., Seefeld, S., 1997. A new mechanism for regional atmospheric chemistry modeling. *J. Geophys. Res.-Atmos.* 102, 25847–25879.
- Sulaymon, I.D., Zhang, Y., Hopke, P.K., Hu, J., Zhang, Y., Li, L., Mei, X., Gong, K., Shi, Z., Zhao, B., Zhao, F., 2021. Persistent high PM<sub>2.5</sub> pollution driven by unfavorable meteorological conditions during the COVID-19 lockdown period in the Beijing-Tianjin-Hebei region, China. *Environ. Res.* 198, 111186.
- Sun, L., Du, J., Li, Y., 2021. A new method for dividing the scopes and priorities of air pollution control based on environmental justice. *Environ. Sci. Pollut. Res.* 28, 12858–12869.
- Wagstrom, K.M., Pandis, S.N., Yarwood, G., Wilson, G.M., Morris, R.E., 2008. Development and application of a computationally efficient particulate matter apportionment algorithm in a three-dimensional chemical transport model. *Atmos. Environ.* 42 (22), 5650–5659.
- Walcek, C.J., Aleksic, N.M., 1998. A simple but accurate mass conservative, peakpreserving mixing ratio bounded advection algorithm with Fortran code. *Atmos. Environ.* 32, 3863–3880.
- Wang, H., Zhao, L., 2018. A joint prevention and control mechanism for air pollution in the Beijing-Tianjin-Hebei region in China based on long-term and massive data mining of pollutant concentration. *Atmos. Environ.* 174, 25–42.
- Wang, Z., Li, J., Wang, Z., Yang, W., Tang, X., Ge, B., Yan, P., Zhu, L., Chen, X., Chen, H., Wand, W., Li, J., Liu, B., Wang, X., Wand, W., Zhao, Y., Lu, N., Su, D., 2014. Modeling study of regional severe hazes over mid-eastern China in January 2013 and its implications on pollution prevention and control. *Sci. China Earth Sci.* 57 (1), 3–13.

- Wang, Y., Yuan, Y., Wang, Q., Liu, C., Zhi, Q., Cao, J., 2020a. Changes in air quality related to the control of coronavirus in China: Implications for the traffic and industrial emission. *Sci. Total Environ.* 731, 139133.
- Wang, P., Chen, K., Zhu, S., Wang, P., Zhang, H., 2020b. Severe air pollution events not avoided by reduced anthropogenic activities during COVID-19 outbreak. *Res. Conserv. Recy.* 148, 104814.
- Wang, Y., Shi, M., Lv, Z., Liu, H., He, K., 2021a. Local and regional contributions to PM<sub>2.5</sub> in the Beijing 2022 Winter Olympics infrastructure areas during haze episodes. *Front. Environ. Sci. Eng.* 15 (6), 140.
- Wang, Z., Uno, I., Yumimoto, K., Itahashi, S., Chen, X., Yang, W., Wang, Z., 2021b. Impacts of COVID-19 lockdown, Spring Festival and meteorology on the NO<sub>2</sub> variations in early 2020 over China based on in-situ observations, satellite retrievals and model simulations. *Atmos. Environ.* 244, 117972.
- WHO, 2006. WHO Air Quality Guidelines for Particulate Matter, Ozone, Nitrogen Dioxide and Sulfur Dioxide: Global Update 2005. World Health Organization.
- Wu, J., Wang, Z., Wang, Q., Li, J., Xu, J., Chen, H., Ge, B., Zhou, G., Chang, L., 2017. Development of an on-line source-tagged model for sulfate, nitrate and ammonium: a modeling study for highly polluted periods in Shanghai, China. *Environ. Pollut.* 221, 168–179.
- Wu, W., Zhang, M., Ding, Y., 2020. Exploring the effect of economic and environment factors on PM2.5 concentration: a case study of the Beijing-Tianjin-Hebei region. *J. Environ. Manag.* 268, 110703.
- Xiao, C., Chang, M., Guo, P., Gu, M., Li, Y., 2020. Analysis of air quality characteristics of Beijing-Tianjin-Hebei and its surrounding air pollution transport channel cities in China. *J. Environ. Sci.* 87, 213–227.
- Xie, Y., Zhao, L., Xue, J., Gao, H., Li, H., Jiang, R., Liu, X., Zhang, S., 2018. Methods for defining the scopes and priorities for joint prevention and control of air pollution regions based on data-mining technologies. *J. Clean. Prod.* 185, 912–921.
- Xu, Y., Xue, W., Lei, Y., Huang, Q., Cheng, S., Ren, Z., Wang, J., 2020. Spatiotemporal variation in the impact of meteorological conditions on PM<sub>2.5</sub> pollution in China from 2000 to 2017. *Atmos. Environ.* 223, 117215.
- Yang, W., Yuan, G., Han, J., 2019. Is China's air pollution control policy effective? Evidence from Yangtze River Delta cities. *J. Clean. Prod.* 220, 110–133.
- Zaveri, R., Peters, L., 1999. A new lumped structure photochemical mechanism for large-scale application. *J. Geophys. Res.-Atmos.* 104, 30387–30415.
- Zhai, S., Jacob, D.J., Wang, X., Shen, L., Li, K., Zhang, Y., Gui, K., Zhao, T., Liao, H., 2019. Fine particulate matter (PM<sub>2.5</sub>) trends in China, 2013–2018: separating contributions from anthropogenic emissions and meteorology. *Atmos. Chem. Phys.* 19, 11031–11041.
- Zhang, Q., Zheng, Y., Tong, D., Shao, M., Wang, S., Zhang, Y., Xu, X., Wang, J., He, H., Liu, W., Ding, Y., Lei, Y., Li, J., Wang, Z., Zhang, X., Wang, Y., Cheng, J., Liu, Y., Shi, Q., Yan, L., Geng, G., Hong, C., Li, M., Liu, F., Zheng, B., Cao, J., Ding, A., Gao, J., Fu, Q., Huo, J., Liu, B., Liu, Z., Yang, F., He, K., Hao, J., 2019. Drivers of improved PM<sub>2.5</sub> air quality in China from 2013 to 2017. *Proc. Natl. Acad. Sci. U. S. A.* 116, 24463–24469.
- Zhang, N., Guan, Y., Li, Y., Wang, S., 2021. New region demarcation method for implementing the Joint Prevention and Control of Atmospheric Pollution policy in China. *J. Clean. Prod.* 325, 129345.
- Zhang, Y., Pan, X., Tian, Y., Liu, H., Chen, X., Ge, B., Wang, Z., Tang, X., Lei, S., Yao, W., Ren, Y., Tian, Y., Li, J., Fu, P., Xin, J., Sun, Y., Cao, J., Wang, Z., 2022. Transport patterns and potential sources of atmospheric pollution during the XXIV Olympic Winter Games period. *Adv. Atmos. Sci.* 39, 1608–1622.
- Zheng, B., Tong, D., Li, M., Liu, F., Hong, C., Geng, G., Li, H., Li, X., Peng, L., Qi, J., Yan, L., Zhang, Y., Zhao, H., Zheng, Y., He, K., Zhang, Q., 2018. Trends in China's anthropogenic emissions since 2010 as the consequence of clean air actions. *Atmos. Chem. Phys.* 18 (19), 14095–14111.
- Zheng, B., Zhang, Q., Geng, G., Chen, C., Shi, Q., Cui, M., Lei, Y., He, K., 2021. Changes in China's anthropogenic emissions and air quality during the COVID-19 pandemic in 2020. *Earth Syst. Sci. Data* 13, 2895–2907.